ATLAS NOTE

ATLAS-CONF-2012-073

June 28, 2012

Search for direct top squark pair production in final states with one isolated lepton, jets, and missing transverse momentum in $\sqrt{s} = 7$ TeV pp collisions using 4.7 fb^{-1} of ATLAS data

The ATLAS Collaboration

ATLAS-CONF-2012-073
06 July 2012

Abstract

A search is presented for direct top squark pair production in final states with one isolated electron or muon, jets, and missing transverse momentum in proton-proton collisions at a center-of-mass energy of 7 TeV. The measurement is based on 4.7 fb^{-1} of data collected with the ATLAS detector at the LHC. The top squarks are assumed to decay each to a top quark and the lightest supersymmetric particle (LSP). The data are found to be consistent with Standard Model expectations. Top squark masses between 230 and 440 GeV are excluded at 95% confidence for massless LSPs, and top squark masses around 400 GeV are excluded for LSP masses up to 125 GeV.

1 Introduction

Weak scale Supersymmetry (SUSY) [1–9] is an extension to the Standard Model (SM) that provides a solution to the hierarchy problem by introducing supersymmetric partners of all SM particles. In the framework of a generic R-parity conserving minimal supersymmetric extension of the SM (MSSM) [10–14], SUSY particles are produced in pairs, and the lightest supersymmetric particle (LSP) is stable and can be a dark matter candidate. In a large variety of models, the LSP is the lightest neutralino, $\tilde{\chi}_1^0$, which only interacts weakly and thus escapes detection.

Light top squarks (stop) are suggested by naturalness arguments [15–18]. In this analysis, one stop mass eigenstate ($\tilde{t}_1$) is assumed to be significantly lighter than the other squarks. A search is presented for directly pair-produced stops, which are each assumed to decay to a top quark and the LSP. The final state for such a signal is characterized by a top quark pair ($t\bar{t}$) produced in association with large missing transverse momentum (the magnitude of which is referred to as $E_{\mathrm{T}}^{\mathrm{miss}}$) from the undetected LSPs.

Searches for direct stop pair production have been previously reported by the CDF and D0 experiments assuming different SUSY mass spectra and decay modes (see for example Ref. [19] and [20]). Searches for stops via $\tilde{g}\tilde{g}$ production have been reported by the ATLAS [21–23] and CMS [24, 25] collaborations.

The ATLAS detector [26] has a solenoid, surrounding the inner tracking detector (ID), and a barrel and two endcap toroidal magnets supporting the muon spectrometer. The ID consists of silicon pixel, silicon microstrip, and transition radiation detectors and provides precision tracking of charged particles for pseudorapidity $|\eta| < 2.5$ [1]. The calorimeter placed outside the solenoid covers $|\eta| < 4.9$ and is composed of sampling electromagnetic and hadronic calorimeters with either liquid argon (LAr) or scintillating tiles as the active media. The muon spectrometer surrounds the calorimeters and consists of a system of precision tracking chambers in $|\eta| < 2.7$, and detectors for triggering in $|\eta| < 2.4$.

The analysis is based on data recorded by the ATLAS detector in 2011 corresponding to 4.7 fb^{-1} of integrated luminosity with the LHC operating at a pp center-of-mass energy of 7 TeV. The data were collected using a logical OR of a $E_{\mathrm{T}}^{\mathrm{miss}}$ and a single lepton (electron or muon) trigger. The combined triggers reach plateau efficiencies >98% for the chosen selection criteria on $E_{\mathrm{T}}^{\mathrm{miss}}$ and the leptons. Requirements that ensure the quality of beam conditions, detector performance and data are imposed.

2 Signal and Background Simulation

Monte Carlo (MC) event samples with full ATLAS detector simulation [27] based on the `Geant4` program [28] are used to aid in the description of the background and to model the SUSY signal. The effect of multiple pp interactions per bunch crossing is also simulated. Production of top quark pairs is simulated with `MC@NLO 4.01` [29, 30], alternatively using `ALPGEN 2.14` [31] and `PowHeg HVQ patch 4` [32–34]. The data modeling is improved for high jet multiplicities by reweighting the `MC@NLO` sample to match the jet multiplicity distribution in `ALPGEN 2.14`. `AcerMC 3.7` [35] samples with various parameter settings are used to assess the uncertainties associated with initial and final state radiation (ISR/FSR) [36]. A top quark mass of 172.5 GeV is used consistently. W and Z/γ^* production in association with jets are each modeled with `ALPGEN`. Diboson VV (WW, WZ, ZZ) production is simulated with `ALPGEN` and cross-checked with `HERWIG 6.520` [37]. Single top production is modeled with `MC@NLO`, and $t\bar{t}$ events produced in association with Z, W or WW ($t\bar{t}+V$) are generated with `MADGRAPH 5` [38]. Next-to-leading order (NLO) PDFs `CT10` [39] are used with all NLO MC samples. For all other sam-

[1] ATLAS uses a right-handed coordinate system with its origin at the nominal interaction point in the centre of the detector and the z-axis along the beam pipe. Cylindrical coordinates (r, ϕ) are used in the transverse plane, ϕ being the azimuthal angle around the beam pipe. The pseudorapidity η is defined in terms of the polar angle θ by $\eta = -\ln\tan(\theta/2)$, and $\Delta R = \sqrt{(\Delta\eta)^2 + (\Delta\phi)^2}$

ples, LO PDFs are used: MRSTmcal [40] with HERWIG, and CTEQ6L1 [41] with ALPGEN and MADGRAPH. Fragmentation and hadronisation for the ALPGEN and MC@NLO samples are performed with HERWIG, using JIMMY 4.31 [42] for the underlying event, and for the MADGRAPH samples PYTHIA 6.425 [43] is used. The $t\bar{t}$, single top and $t\bar{t}+V$ production cross sections are normalized to approximate next-to-next-to-leading order (NNLO) [44], next-to-next-to-leading-logarithmic accuracy (NLO+NNLL) [45–47] and NLO [48] calculations, respectively. QCD NNLO FEWZ [49] inclusive W and Z cross sections are used for the normalization of the W+jets and Z+jets processes. Expected diboson yields are normalized using NLO QCD predictions obtained with MCFM [50, 51].

Stop pair production is modeled using HERWIG++ 2.5.2 [52]. A signal grid is generated with a step size of 50 GeV both for the stop and LSP mass values. Signal cross sections are calculated to NLO in the strong coupling constant, including the resummation of soft gluon emission at next-to-leading-logarithmic accuracy (NLO+NLL) [53–55]. The nominal cross section and the uncertainty are taken from an envelope of cross section predictions using different PDF sets and factorisation and renormalisation scales, as described in Ref. [56].

3 Event Selection and Reconstruction

Events must pass basic quality criteria to reject detector noise and non-collision backgrounds [57,58] and are required to have ≥ 1 reconstructed primary vertex associated with five or more tracks with transverse momentum $p_{\mathrm{T}} > 0.4$ GeV. Events are retained if they contain exactly one muon [59] with $|\eta| < 2.4$ and $p_{\mathrm{T}} > 20$ GeV or one electron passing 'tight' [60] selection criteria with $|\eta| < 2.47$ and $p_{\mathrm{T}} > 25$ GeV. Leptons are required to be isolated from other particles. The scalar sum of the transverse momenta of tracks above 1 GeV within a cone of size $\Delta R < 0.2$ around the lepton candidate is required to be $< 10\%$ of the electron p_{T}, and < 1.8 GeV for the muon. Events are rejected if they contain additional leptons passing looser selection criteria [61]. Jets are reconstructed from three-dimensional calorimeter energy clusters using the anti-k_t jet clustering algorithm [62] with a radius parameter of 0.4. The jet energy is corrected for the effects of calorimeter non-compensation and inhomogeneities by using p_{T}- and η-dependent calibration factors based on MC simulations and validated with extensive test-beam and collision-data studies [63]. To suppress jet background originating from uncorrelated soft collisions, $\geq 75\%$ of the summed p_{T} of all tracks associated to a jet must come from tracks associated to the selected primary vertex. Events with four or more jets are selected with $|\eta| < 2.5$ and $p_{\mathrm{T}} > 80, 60, 40, 25$ GeV, respectively. At least one jet needs to be identified as a b-jet. Jets containing a b-hadron decay (b-jets) are identified using the 'MV1' b-tagging algorithm [64] which exploits both impact parameter and secondary vertex information. An operating point is employed corresponding to an average 75% b-tagging efficiency and a $< 2\%$ misidentification rate for light-quark/gluon jets for jets with $p_{\mathrm{T}} > 20$ GeV and $|\eta| < 2.5$ in $t\bar{t}$ MC events.

Ambiguities between overlapping objects are resolved by discarding either jet or lepton candidates [61] based on their distance ΔR. The measurement of $E_{\mathrm{T}}^{\mathrm{miss}}$ is based on the transverse momenta of all electron and muon candidates, all jets after overlap removal, and all calorimeter energy clusters not associated to such objects. The background is reduced by requiring $\Delta\phi_{\mathrm{min}} > 0.8$, where $\Delta\phi_{\mathrm{min}}$ is defined by the minimum azimuthal separation between the two highest p_{T} jets and the missing transverse momentum direction. A selection on the jet-jet-jet mass m_{jjj} of the hadronically decaying top quark is required to specifically reject the dileptonic $t\bar{t}$ background, where both W bosons from the top quarks decay leptonically. The jet-jet pair having invariant mass > 60 GeV which has the smallest ΔR is selected to form the hadronic W boson. The mass m_{jjj} is reconstructed from a third jet closest in ΔR to the hadronic W boson momentum vector and 130 GeV $< m_{jjj} <$ 205 GeV is required.

3.1 Signal Regions

Five signal regions (SR A - E) are defined in order to optimize the sensitivity for different stop and LSP masses. For increasing stop mass and increasing mass difference between stop and LSP the requirements are tightened on $E_{\mathrm{T}}^{\mathrm{miss}}$, on the ratio $E_{\mathrm{T}}^{\mathrm{miss}}/\sqrt{H_{\mathrm{T}}}$, where H_{T} is the scalar sum of the momenta of the four selected jets, and on the transverse mass m_{T},[2] as shown in Table 1. The numbers of observed events in each signal region after applying all selection criteria are given in Table 2.

Table 1: Selection requirements defining the SR A - E.

Requirement	SR A	SR B	SR C	SR D	SR E
$E_{\mathrm{T}}^{\mathrm{miss}}$ [GeV] >	150	150	150	225	275
$E_{\mathrm{T}}^{\mathrm{miss}}/\sqrt{H_{\mathrm{T}}}$ [GeV$^{1/2}$] >	7	9	11	11	11
m_{T} [GeV] >	120	120	120	130	140

The product of the kinematic acceptance and detector efficiency ($A \cdot \epsilon$) varies between 5% and 1% for SR A and between 3% and 0.1% for SR E as the stop-LSP mass difference varies between 600 and 300 GeV.

3.2 Background Modeling

The dominant background arises from dileptonic $t\bar{t}$ events in which one of the leptons is not identified, is outside the detector acceptance, or is a hadronically decaying τ lepton. In all these cases, the $t\bar{t}$ decay products include two or more high-p_{T} neutrinos, resulting in large $E_{\mathrm{T}}^{\mathrm{miss}}$ and m_{T}. Three control regions enriched in dileptonic $t\bar{t}$ events (*2-lep TR*), single-leptonic $t\bar{t}$ events (*1-lep TR*), and W+jets events (*1-lep WR*) are designed to normalize the corresponding backgrounds using data. The *2-lep TR* differs from the signal regions by selecting events with exactly two leptons, applying no requirements on m_{T}, $E_{\mathrm{T}}^{\mathrm{miss}}/\sqrt{H_{\mathrm{T}}}$ and m_{jjj}, and by requiring $E_{\mathrm{T}}^{\mathrm{miss}} > 125$ GeV. The *1-lep TR* and *1-lep WR* have selection criteria identical to SR A, except for the m_{T} requirement which is changed to 60 GeV $< m_{\mathrm{T}} <$ 90 GeV. The *1-lep WR* also has a *b*-jet veto instead of a *b*-jet requirement. Top production accounts for > 90% of events in the top control regions and W+jets production for > 50% in the W control region. The maximum signal contamination is < 10%.

A simultaneous fit to the numbers of observed events in the three control regions and one signal region at a time is performed to normalize the $t\bar{t}$ and W+jets background estimates as well as determine or limit a potential signal contribution. The *1-lep* and *2-lep TR* have $t\bar{t}$ normalizations that float independently and that are found to be in good agreement. The multijet background which mainly originates from jets misidentified as leptons is estimated using the matrix method [61]. Other background contributions (VV, $t\bar{t}+V$, single top) are estimated using MC simulation normalized to the theory cross sections. The Z+jets background is found to be negligible. Systematic uncertainties are treated as nuisance parameters with Gaussian probability density functions.

Good agreement is observed between data and the SM prediction before the fit as shown in Figure 1 for the $E_{\mathrm{T}}^{\mathrm{miss}}$ distributions in the *2-lep TR*, and the m_{T} distribution for the looser requirement $E_{\mathrm{T}}^{\mathrm{miss}} >$ 40 GeV and no requirements on $E_{\mathrm{T}}^{\mathrm{miss}}/\sqrt{H_{\mathrm{T}}}$ and m_{jjj}, as well as for the $E_{\mathrm{T}}^{\mathrm{miss}}$ distribution in SR A.

[2] m_{T} is defined as $m_{\mathrm{T}}^2 = 2p_{\mathrm{T}}^{\mathrm{lep}}E_{\mathrm{T}}^{\mathrm{miss}}(1-\cos(\Delta\phi))$, where $\Delta\phi$ is the azimuthal angle between the lepton and missing momentum direction.

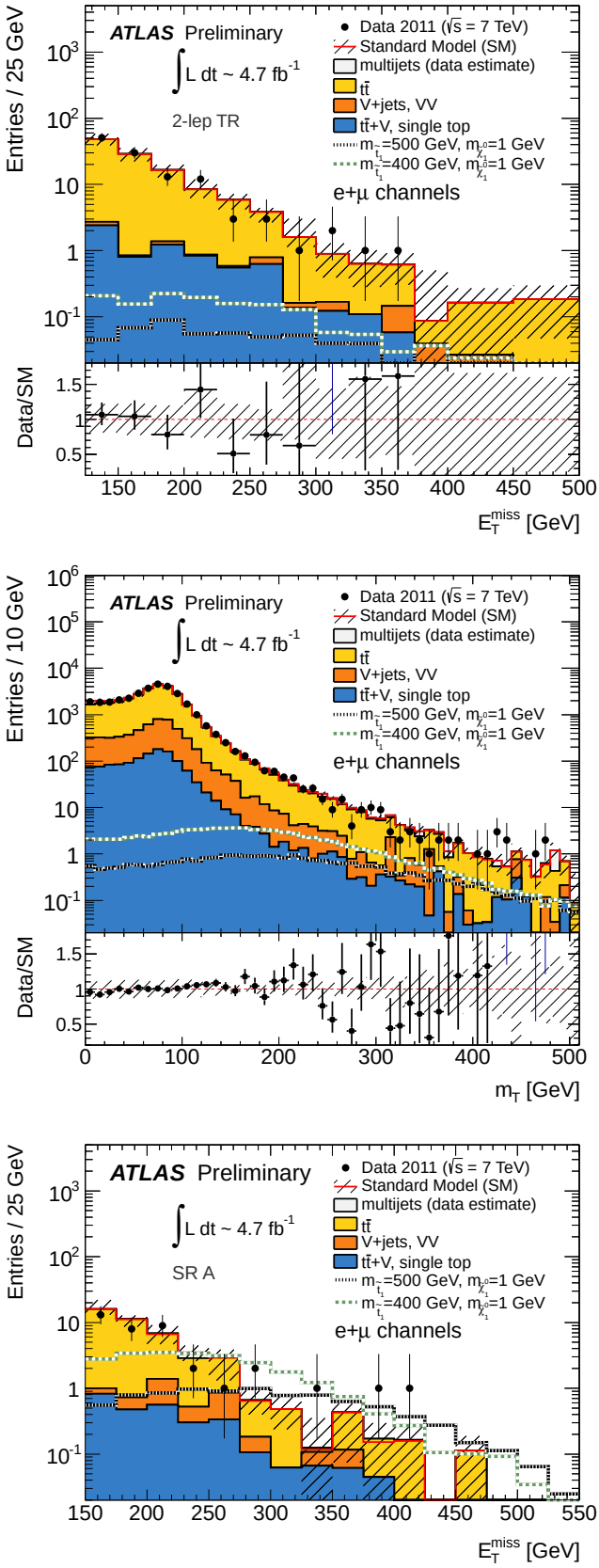

Figure 1: Top: $E_{\mathrm{T}}^{\mathrm{miss}}$ distributions for the *2-lep TR*. Center: m_{T} distribution for looser requirements (see text). Bottom: $E_{\mathrm{T}}^{\mathrm{miss}}$ distributions for SR A. All plots show the combined electron and muon channels. Hatched areas indicate the combined uncertainty due to MC statistics and the jet energy scale.

Table 2: Numbers of observed events in the five signal regions and three background control regions, as well as their estimated values and all (statistic and systematic) uncertainties from a fit to the control regions only, for the combined electron and muon channels. The expected numbers of signal events for $m_{\tilde{t}_1}$ = 400 GeV (500 GeV) and $m_{\tilde{\chi}_1^0}$ = 1 GeV for benchmark points 1 (2) are listed for comparison. The central values of the fitted sum of backgrounds in the control regions agree with the observations by construction. Furthermore, p_0-values and 95% CL_s observed (expected) upper limits on beyond-SM events, obtained from fits to each signal regions and the control regions, are given.

Regions	SR A	SR B	SR C	SR D	SR E	*2-lep TR*	*1-lep TR*	*1-lep WR*
$t\bar{t}$	36 ± 5	27 ± 4	11 ± 2	4.9 ± 1.3	1.3 ± 0.6	109 ± 10	364 ± 23	59 ± 19
$t\bar{t}+V$, single top	2.9 ± 0.7	2.5 ± 0.6	1.6 ± 0.3	0.9 ± 0.3	0.4 ± 0.1	7.2 ± 1.3	18 ± 3	6.1 ± 1.6
V+jets, VV	2.5 ± 1.3	1.7 ± 0.8	0.4 ± 0.1	0.3 ± 0.1	0.1 ± 0.1	1.6 ± 0.8	38 ± 11	162 ± 23
Multijet	$0.4^{+0.4}_{-0.4}$	$0.3^{+0.3}_{-0.3}$	$0.3^{+0.3}_{-0.3}$	$0.3^{+0.3}_{-0.3}$	$0.0^{+0.3}_{-0.0}$	$0.0^{+0.6}_{-0.0}$	1.7 ± 1.7	0.8 ± 0.8
Total background	42 ± 6	31 ± 4	13 ± 2	6.4 ± 1.4	1.8 ± 0.7	118 ± 10	421 ± 20	228 ± 15
Signal benchmark 1 (2)	25.6 (8.8)	23.0 (8.1)	17.5 (6.9)	13.5 (6.2)	7.1 (4.5)	1.7 (0.6)	2.3 (0.6)	0.4 (0.1)
Observed events	38	25	15	8	5	118	421	228
p_0-values	0.5	0.5	0.32	0.24	0.015	-	-	-
Obs. (exp.) $N_{\text{beyond-SM}} <$	15.1 (17.2)	10.1 (13.8)	10.8 (9.2)	8.4 (7.0)	8.2 (4.6)	-	-	-

4 Systematics

The dominant sources of systematic uncertainties in the fitted $t\bar{t}$ background estimate arise from theoretical and MC modeling uncertainties. They are determined by using different generators (`MC@NLO`, `PowHeg` and `ALPGEN`), different showering models (`HERWIG` and `PYTHIA`) and by varying ISR/FSR parameters, and amount to 10%-30% on the extrapolation from the control to the various signal regions. Electroweak single top production is associated with an 8% theory uncertainty [45–47] and $t\bar{t}+V$ background with a 30% uncertainty [48]. The difference between `ALPGEN` and `HERWIG` is used to assess the uncertainty on the diboson background, and the uncertainty on the multijet background is based on the matrix method. Both are assigned an uncertainty of 100%.

Experimental uncertainties affect the signal and background yields estimated from MC events and are dominated by the uncertainties in jet energy scale, jet energy resolution and b-tagging. Uncertainties related to the trigger and lepton reconstruction and identification (momentum and energy scales, resolutions and efficiencies) give smaller contributions. Other small uncertainties are due to modeling of multiple pp interactions, the integrated luminosity (3.9% [65, 66]), and the limited MC and data statistics. As the stop-LSP mass difference varies between 600 and 300 GeV the uncertainty on $A \cdot \epsilon$ varies between 7% and 20%.

5 Results

Table 2 shows the results of the background fit to the control regions, extrapolated to the signal regions. The fitted W+jets and $t\bar{t}$ backgrounds are compatible with MC predictions. To assess the agreement between SM expectation and observation in the signal regions a simultaneous fit including signal and control regions is performed. The p_0-values obtained are given in Table 2. No significant excess of events is found.

One-sided exclusion limits are derived using the CL_s method [67], based on the same simultaneous fit (including signal and control regions) but taking the predicted signal contamination in the control

regions into account. To obtain the best expected combined exclusion limit, a mapping in the stop-LSP mass plane is constructed by selecting the signal region with the lowest expected CL_s value for each grid point. The expected and observed 95% CL_s exclusion limits are displayed in Figure 2. Stop masses are excluded between 230 and 440 GeV for massless LSPs, and stop masses around 400 GeV are excluded for LSP masses up to 125 GeV. This significantly extends previous stop mass limits.

Limits on beyond-SM contributions are derived from the same simultaneous fit but without signal model-dependent inputs (i.e. without signal contamination in the control regions, and without experimental and theoretical signal systematic uncertainties). The resulting limits are shown in the bottom of Table 2.

6 Conclusion

In summary, a search for stop pair production is presented in final states with one isolated lepton, jets, and missing transverse momentum in $\sqrt{s}$ = 7 TeV pp collisions corresponding to 4.7 fb^{-1} of ATLAS 2011 data. The stops are assumed to decay each to a top quark and a long-lived undetected neutral particle. No significant excess of events above the rate predicted by the Standard Model is observed and 95% CL_s upper limits are set on the stop mass in the stop-LSP mass plane, significantly extending previous stop mass limits.

References

[1] H. Miyazawa, *Baryon Number Changing Currents*, Prog. Theor. Phys. **36 (6)** (1966) 1266–1276.

[2] R. Ramond, *Dual Theory for Free Fermions*, Phys. Rev. **D3** (1971) 2415–2418.

[3] Y. Golfand and E. Likhtman, *Extension of the Algebra of Poincare Group Generators and Violation of p Invariance*, JETP Lett. **13** (1971) 323–326.

[4] A. Neveu and J. Schwarz, *Factorizable dual model of pions*, Nucl. Phys. **B31** (1971) 86–112.

[5] A. Neveu and J. Schwarz, *Quark Model of Dual Pions*, Phys. Rev. **D4** (1971) 1109–1111.

[6] J. Gervais and B. Sakita, *Field theory interpretation of supergauges in dual models*, Nucl. Phys. **B34** (1971) 632–639.

[7] D. Volkov and V. Akulov, *Is the Neutrino a Goldstone Particle?*, Phys. Lett. **B46** (1973) 109–110.

[8] J. Wess and B. Zumino, *A Lagrangian Model Invariant Under Supergauge Transformations*, Phys. Lett. **B49** (1974) 52.

[9] J. Wess and B. Zumino, *Supergauge Transformations in Four-Dimensions*, Nucl. Phys. **B70** (1974) 39–50.

[10] P. Fayet, *Supersymmetry and Weak, Electromagnetic and Strong Interactions*, Phys. Lett. **B64** (1976) 159.

[11] P. Fayet, *Spontaneously Broken Supersymmetric Theories of Weak, Electromagnetic and Strong Interactions*, Phys. Lett. **B69** (1977) 489.

[12] G. R. Farrar and P. Fayet, *Phenomenology of the Production, Decay, and Detection of New Hadronic States Associated with Supersymmetry*, Phys. Lett. **B76** (1978) 575–579.

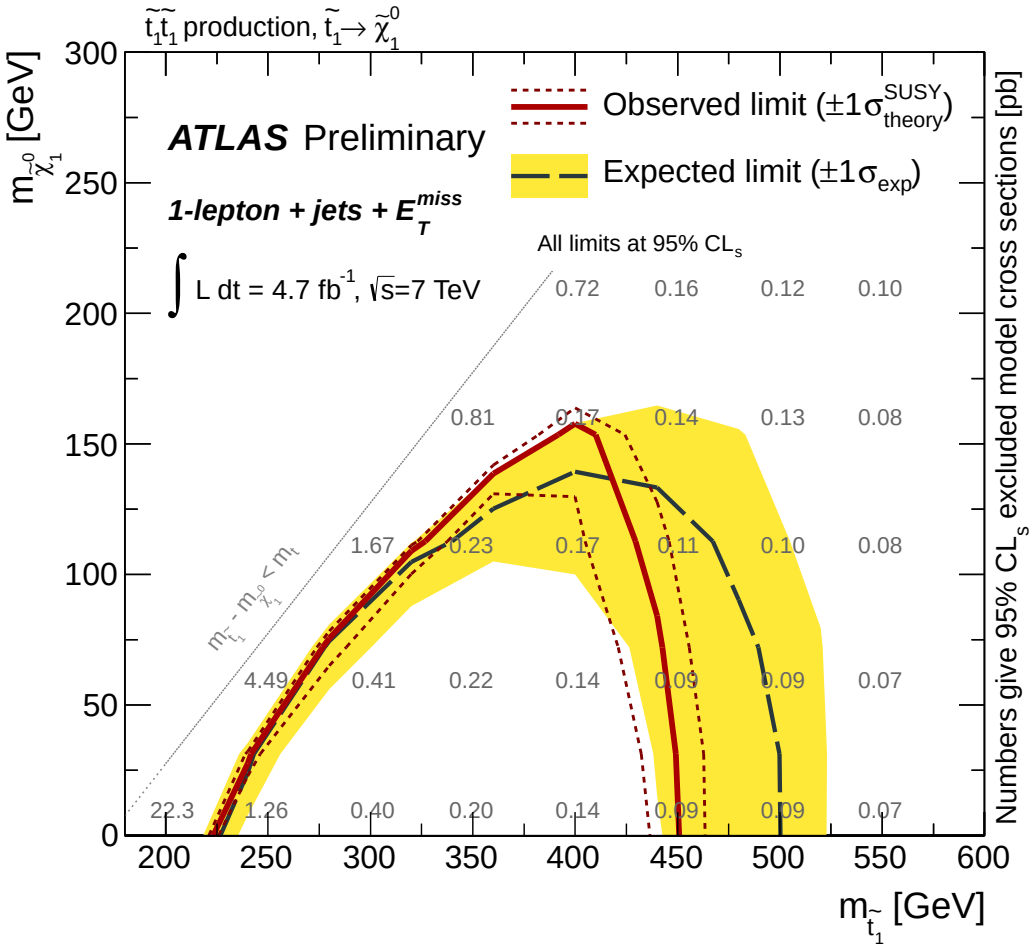

Figure 2: Expected (black dashed) and observed (red solid) 95% CL$_s$ excluded region (under the curve) in the plane of $m_{\tilde{\chi}_1^0}$ vs. $m_{\tilde{t}_1}$, assuming $BR(\tilde{t}_1 \rightarrow t\tilde{\chi}_1^0) = 100\%$. All uncertainties except the theoretical signal cross section uncertainties are included. The contours of the yellow (light grey) band around the expected limit are the $\pm 1\,\sigma$ results. The dotted red lines around the observed limit illustrate the change in the observed limit as the nominal signal cross section is scaled up and down by the theoretical uncertainty. The overlaid numbers give the upper limit on the signal cross section, in pb.

[13] P. Fayet, *Relations Between the Masses of the Superpartners of Leptons and Quarks, the Goldstino Couplings and the Neutral Currents*, Phys. Lett. **B84** (1979) 416.

[14] S. Dimopoulos and H. Georgi, *Softly Broken Supersymmetry and SU(5)*, Nucl. Phys. **B193** (1981) 150.

[15] S. Weinberg, *Implications of Dynamical Symmetry Breaking*, Phys.Rev. **D13** (1976) 974–996.

[16] E. Gildener, *Gauge Symmetry Hierarchies*, Phys.Rev. **D14** (1976) 1667.

[17] S. Weinberg, *Implications of Dynamical Symmetry Breaking: An Addendum*, Phys.Rev. **D19** (1979) 1277–1280.

[18] L. Susskind, *Dynamics of Spontaneous Symmetry Breaking in the Weinberg-Salam Theory*, Phys.Rev. **D20** (1979) 2619–2625.

[19] CDF Collaboration, *Search for Pair Production of Supersymmetric Top Quarks in Dilepton Events from $p\overline{p}$ Collisions at sqrt(s)=1.96 TeV*, Phys. Rev. Lett. **104** (2010) 251801.

[20] D0 Collaboration, *Search for the lightest scalar top quark in events with two leptons in ppbar collisions at sqrt(s)=1.96 TeV*, Phys. Lett. **B675** (2009) 289.

[21] ATLAS Collaboration, *Search for supersymmetry in pp collisions at sqrt(s) = 7 TeV in final states with missing transverse momentum and b-jets with the ATLAS detector*, Phys.Rev.D **85** (2012) 112006, `arXiv:1203.6193 [hep-ex]`.

[22] ATLAS Collaboration, *Search for Gluinos in Events with Two Same-Sign Leptons, Jets, and Missing Transverse Momentum with the ATLAS Detector in pp Collisions at $\sqrt{s} = 7$ TeV*, Phys. Rev. Lett. **108** (2012) 241802.

[23] ATLAS Collaboration, *Hunt for new phenomena using large jet multiplicities and missing transverse momentum with ATLAS in $4.7\,fb^{-1}$ of $\sqrt{s} = 7$ TeV proton-proton collisions*, `arXiv:1206.1760 [hep-ex]`.

[24] CMS Collaboration, *Search for Supersymmetry in Events with b Jets and Missing Transverse Momentum at the LHC*, JHEP **1107** (2011) 113.

[25] CMS Collaboration, *Search for new physics in events with same-sign dileptons and b-tagged jets in pp collisions at $\sqrt{s} = 7$ TeV*, `arXiv:1205.3933 [hep-ex]`.

[26] ATLAS Collaboration, *The ATLAS Experiment at the CERN Large Hadron Collider*, JINST **3** (2008) S08003.

[27] ATLAS Collaboration, *The ATLAS Simulation Infrastructure*, Eur. Phys. J. **C70** (2010) 823–874.

[28] GEANT4 Collaboration, S. Agostinelli et al., *GEANT4: A simulation toolkit*, Nucl. Instrum. Meth. **A506** (2003) 250–303.

[29] S. Frixione, E. Laenen, P. Motylinski, and B. R. Webber, *Single-top production in MC@NLO*, JHEP **03** (2006) 092.

[30] S. Frixione, E. Laenen, P. Motylinski, B. R. Webber, and C. D. White, *Single-top hadroproduction in association with a W boson*, JHEP **07** (2008) 029.

[31] M. L. Mangano, M. Moretti, F. Piccinini, R. Pittau, and A. D. Polosa, *ALPGEN, a generator for hard multiparton processes in hadronic collisions*, JHEP **07** (2003) 001.

[32] P. Nason, *A New method for combining NLO QCD with shower Monte Carlo algorithms*, JHEP **0411** (2004) 040.

[33] S. Frixione, P. Nason, and C. Oleari, *Matching NLO QCD computations with parton shower simulations: the POWHEG method*, JHEP **0711** (2007) 070.

[34] S. Alioli, P. Nason, C. Oleari, and E. Re, *A general framework for implementing NLO calculations in shower Monte Carlo programs: the POWHEG BOX*, JHEP **1006** (2010) 043.

[35] B. P. Kersevan and E. Richter-Was, *The Monte Carlo event generator AcerMC version 2.0 with interfaces to PYTHIA 6.2 and HERWIG 6.5*, arXiv:hep-ph/0405247 [hep-ph].

[36] ATLAS Collaboration, *Measurement of $t\bar{t}$ production with a veto on additional central jet activity in pp collisions at sqrt(s) = 7 TeV using the ATLAS detector*, arXiv:1203.5015 [hep-ex]. CERN-PH-EP-2012-062.

[37] G. Corcella et al., *HERWIG 6.5: an event generator for Hadron Emission Reactions With Interfering Gluons (including supersymmetric processes)*, JHEP **01** (2001) 010.

[38] J. Alwall et al., *MadGraph/MadEvent v4: The New Web Generation*, JHEP **09** (2007) 028.

[39] H.-L. Lai, M. Guzzi, J. Huston, Z. Li, P. M. Nadolsky, et al., *New parton distributions for collider physics*, Phys.Rev. **D82** (2010) 074024.

[40] A. D. Martin, W. J. Stirling, R. S. Thorne, and G. Watt, *Parton distributions for the LHC*, Eur. Phys. J. **C63** (2009) 189.

[41] J. Pumplin et al., *New generation of parton distributions with uncertainties from global QCD analysis*, JHEP **07** (2002) 012.

[42] J. M. Butterworth, J. R. Forshaw, and M. H. Seymour, *Multiparton interactions in photoproduction at HERA*, Z. Phys. **C72** (1996) 637–646.

[43] T. Sjostrand, S. Mrenna, and P. Z. Skands, *PYTHIA 6.4 Physics and Manual*, JHEP **0605** (2006) 026.

[44] M. Aliev, H. Lacker, U. Langenfeld, S. Moch, P. Uwer, et al., *HATHOR: HAdronic Top and Heavy quarks crOss section calculatoR*, Comput.Phys.Commun. **182** (2011) 1034–1046.

[45] N. Kidonakis, *Next-to-next-to-leading-order collinear and soft gluon corrections for t-channel single top quark production*, Phys.Rev. **D83** (2011) 091503.

[46] N. Kidonakis, *Two-loop soft anomalous dimensions for single top quark associated production with a W- or H-*, Phys.Rev. **D82** (2010) 054018.

[47] N. Kidonakis, *NNLL resummation for s-channel single top quark production*, Phys.Rev. **D81** (2010) 054028.

[48] J. M. Campbell and R. K. Ellis, *$t\bar{t}W^{+-}$ production and decay at NLO*, arXiv:1204.5678 [hep-ph].

[49] R. Gavin, Y. Li, F. Petriello, and S. Quackenbush, *FEWZ 2.0: A code for hadronic Z production at next-to- next-to-leading order*, arXiv:1011.3540 [hep-ph].

[50] J. M. Campbell and R. K. Ellis, *An Update on vector boson pair production at hadron colliders*, Phys.Rev. **D60** (1999) 113006.

[51] J. M. Campbell, R. K. Ellis, and C. Williams, *Vector boson pair production at the LHC*, JHEP **1107** (2011) 018.

[52] M. Bahr et al., *Herwig++ Physics and Manual*, Eur. Phys. J. **C58** (2008) 639–707.

[53] W. Beenakker, M. Kramer, T. Plehn, M. Spira, and P. M. Zerwas, *Stop production at hadron colliders*, Nucl. Phys. **B515** (1998) 3–14.

[54] W. Beenakker, S. Brensing, M. Kramer, A. Kulesza, E. Laenen, and I. Niessen, *Supersymmetric top and bottom squark production at hadron colliders*, JHEP. **1008** (2010) 098.

[55] W. Beenakker, S. Brensing, M. Kramer, A. Kulesza, E. Laenen, et al., *Squark and gluino hadroproduction*, Int.J.Mod.Phys. **A26** (2011) 2637–2664.

[56] M. Kramer, A. Kulesza, R. van der Leeuw, M. Mangano, S. Padhi, et al., *Supersymmetry production cross sections in pp collisions at sqrts = 7 TeV*, arXiv:1206.2892 [hep-ph].

[57] ATLAS Collaboration, *Selection of jets produced in proton-proton collisions with the ATLAS detector using 2011 data*, . ATLAS-CONF-2012-020 https://cdsweb.cern.ch/record/1430034.

[58] ATLAS Collaboration, *Studies of the performance of the ATLAS detector using cosmic-ray muons*, Eur. Phys. J. **C71** (2011) 1593.

[59] ATLAS Collaboration. ATLAS-CONF-2011-063 https://cdsweb.cern.ch/record/1345743.

[60] ATLAS Collaboration, *Electron performance measurements with the ATLAS detector using the 2010 LHC proton-proton collision data*, Eur.Phys.J. **C72** (2012) 1909.

[61] ATLAS Collaboration, *Search for supersymmetry in final states with jets, missing transverse momentum and one isolated lepton in* $\sqrt{s} = 7$ *TeV pp collisions using 1* fb^{-1} *of ATLAS data*, Phys. Rev. D **85** (2012) 012006.

[62] M. Cacciari, G. P. Salam, and G. Soyez, *The anti-k_t jet clustering algorithm*, JHEP **04** (2008) 063.

[63] ATLAS Collaboration, *Jet energy measurement with the ATLAS detector in proton-proton collisions at* $\sqrt{s} = 7$ TeV, arXiv:1112.6426 [hep-ex]. CERN-PH-EP-2011-191.

[64] ATLAS Collaboration. ATLAS-CONF-2012-043 https://cdsweb.cern.ch/record/1435197.

[65] ATLAS Collaboration, *Luminosity Determination in pp Collisions at* $\sqrt{s} = 7$ *TeV Using the ATLAS Detector at the LHC*, Eur.Phys.J. **C71** (2011) 1630.

[66] ATLAS Collaboration. ATLAS-CONF-2011-116 http://cdsweb.cern.ch/record/1376384.

[67] A. Read, *Presentation of search results: the CLs technique*, Journal of Physics G: Nucl. Part. Phys. **28** (2002) 2693–2704.

A Additional plots

Figure 3 shows the exclusion limits as obtained per signal region. The mapping of signal region to signal model is illustrated in Figure 4.

Figures 5 to 10 show additional comparisons between data and background expectations. The simulation is normalized as described in the text above. The hatched area in each of the plots indicates the combined uncertainty due to MC statistics and the jet energy scale.

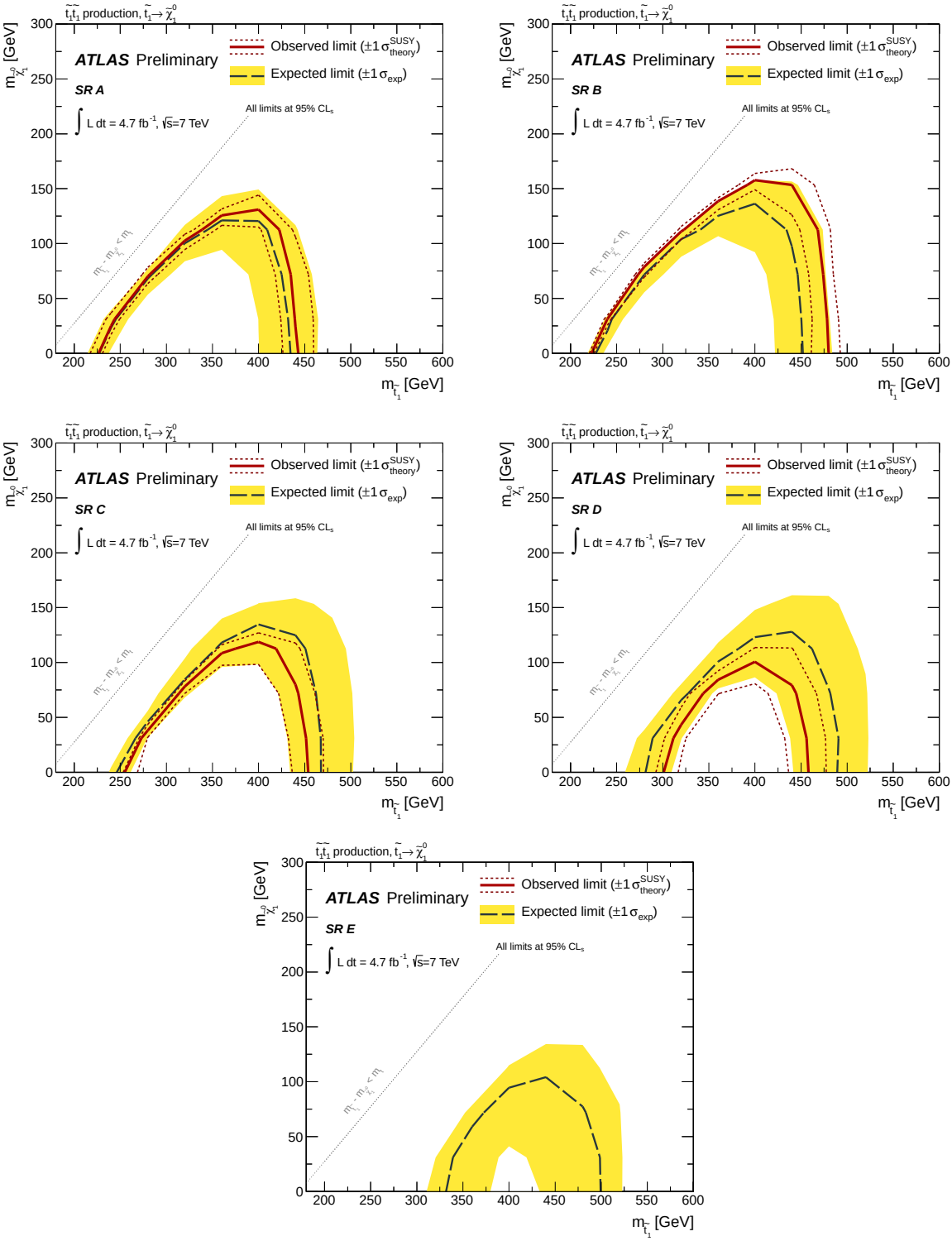

Figure 3: Expected and observed exclusion 95% CL_s exclusion limits for the five individual signal regions (the excluded region is under the curve). Note that in SR E there is no observed exclusion limit due to an excess in data.

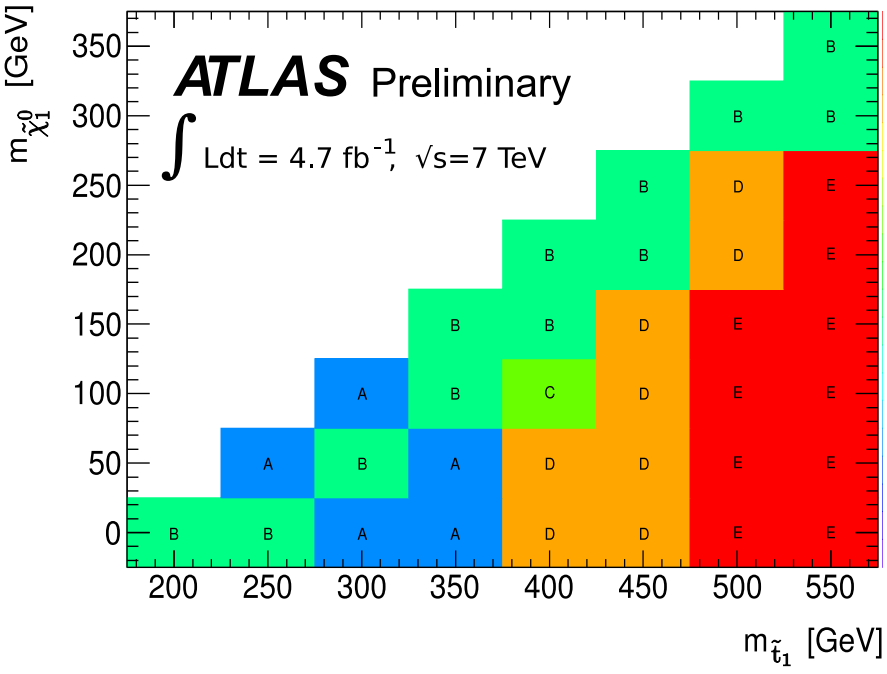

Figure 4: Illustration of the best expected signal region per signal grid point. This mapping is used for the final combined exclusion limits.

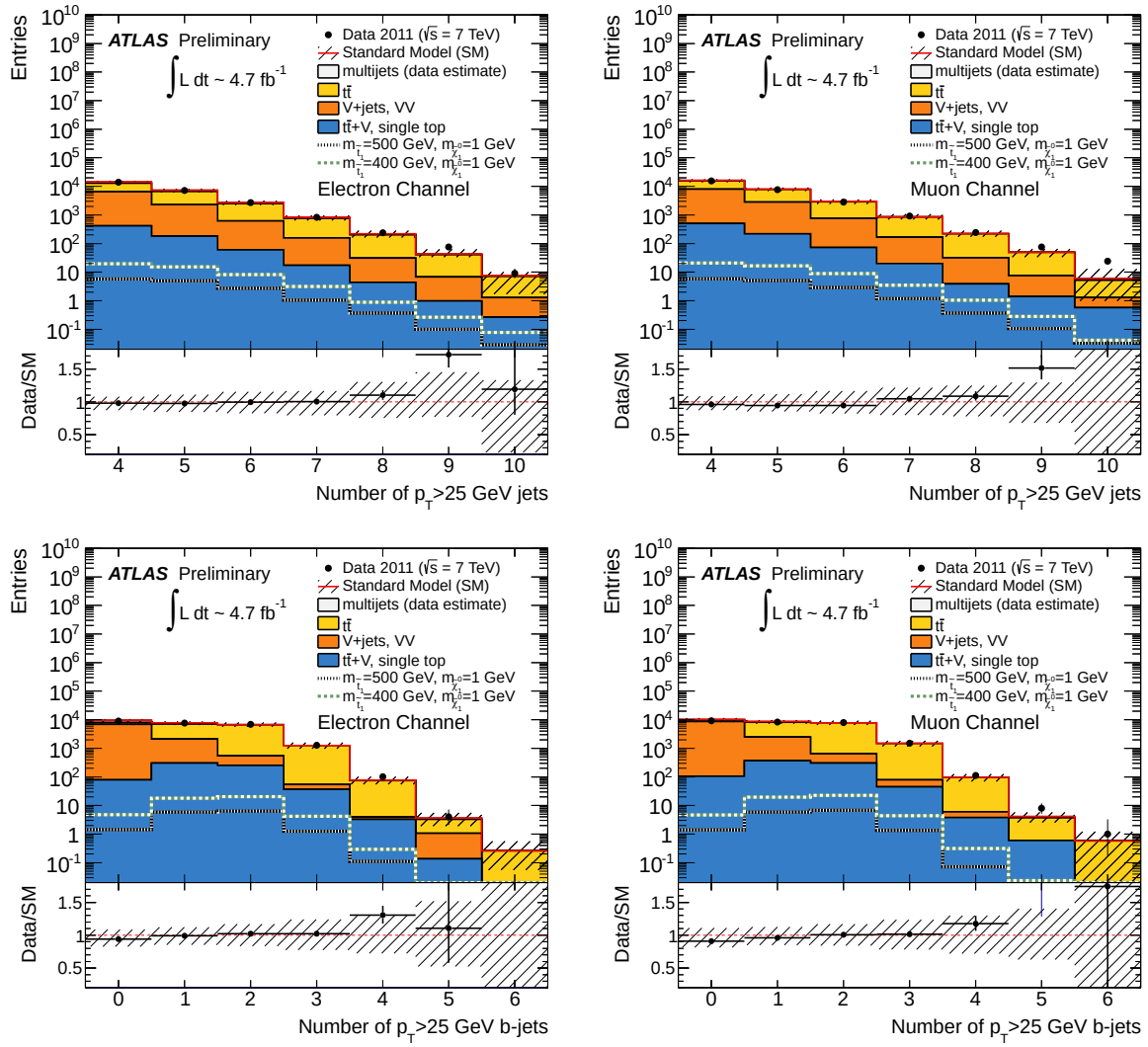

Figure 5: Electron (left) and muon (right) jet multiplicity, and b-jet multiplicity distributions in the top, and bottom panels respectively. All plots are after the kinematic selection of one (signal) lepton, four or more (signal) jets, and $E_{\mathrm{T}}^{\mathrm{miss}} > 40$ GeV.

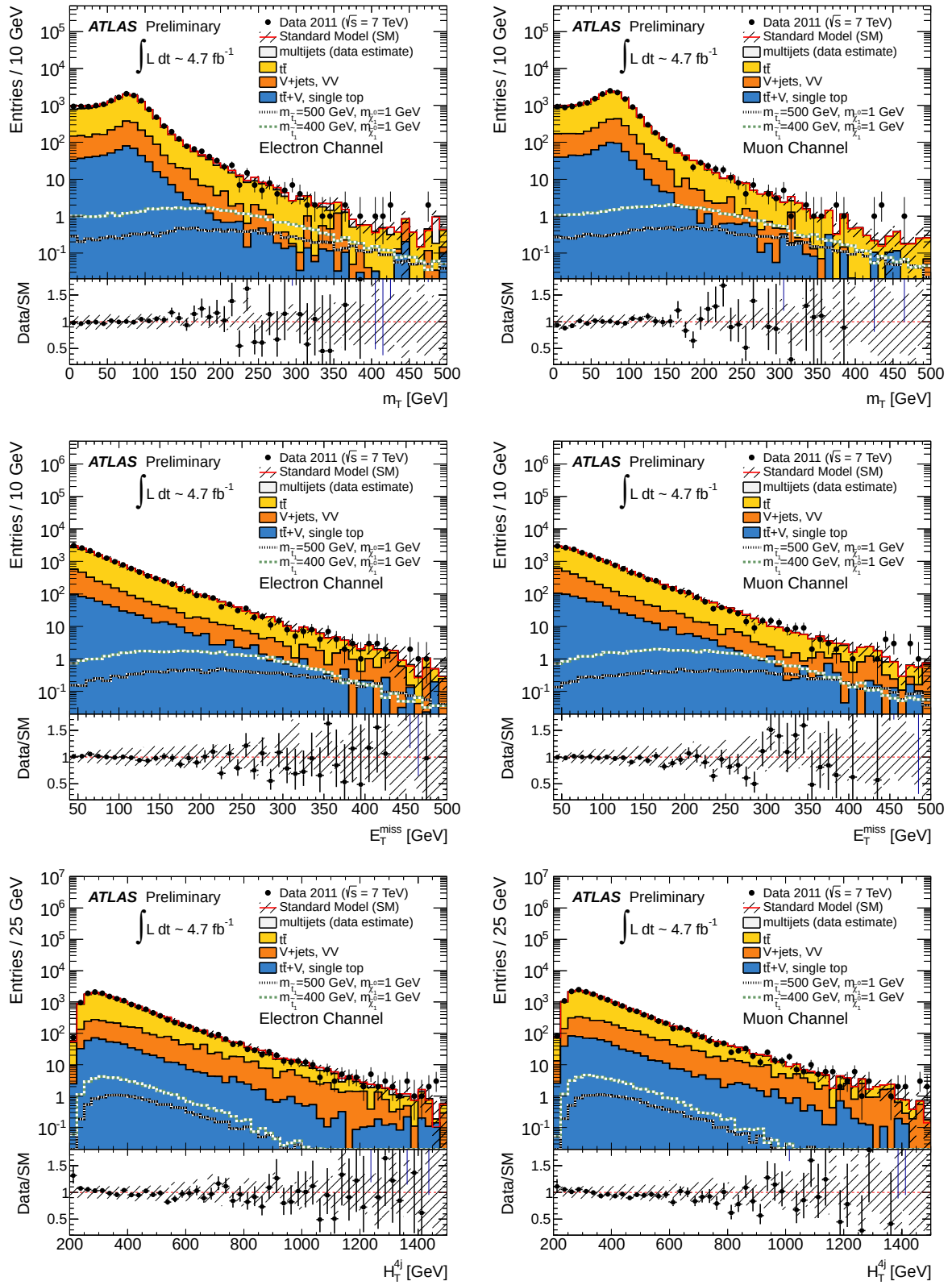

Figure 6: Electron (left) and muon (right) transverse mass (m_{T}), missing transverse momentum ($E_{\mathrm{T}}^{\mathrm{miss}}$), and jet scalar sum ($H_{\mathrm{T}}$) distributions in the top, middle, and bottom panels respectively. All plots are after the kinematic selection of one (signal) lepton, four or more (signal) jets, of which at least one is b-tagged, and $E_{\mathrm{T}}^{\mathrm{miss}} > 40$ GeV.

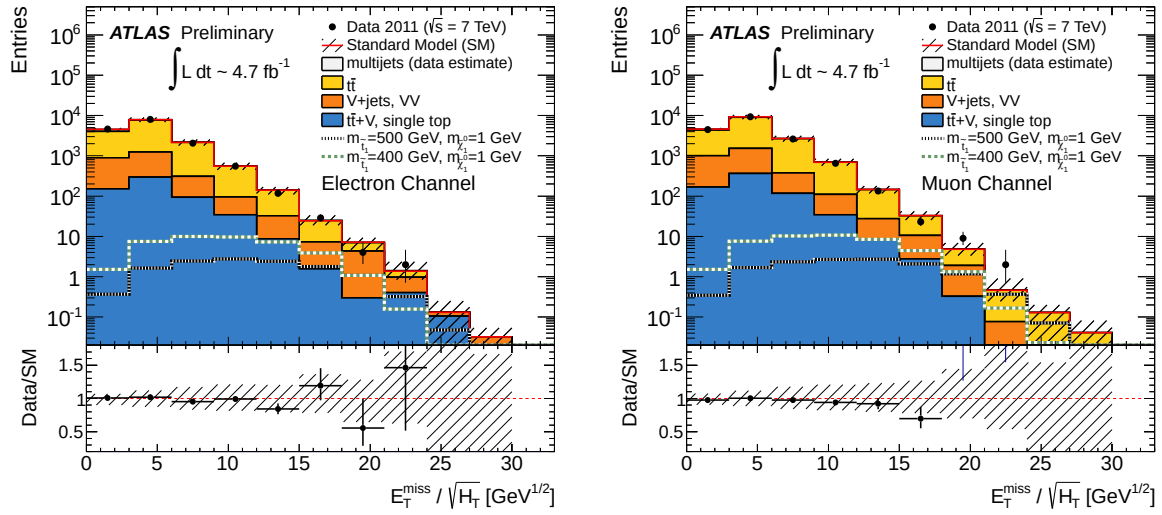

Figure 7: Electron (left) and muon (right) $E_{\mathrm{T}}^{\mathrm{miss}}/\sqrt{H_{\mathrm{T}}}$ distributions. All plots are after the kinematic selection of one (signal) lepton, four or more (signal) jets, of which at least one is b-tagged, and $E_{\mathrm{T}}^{\mathrm{miss}} > 40$ GeV.

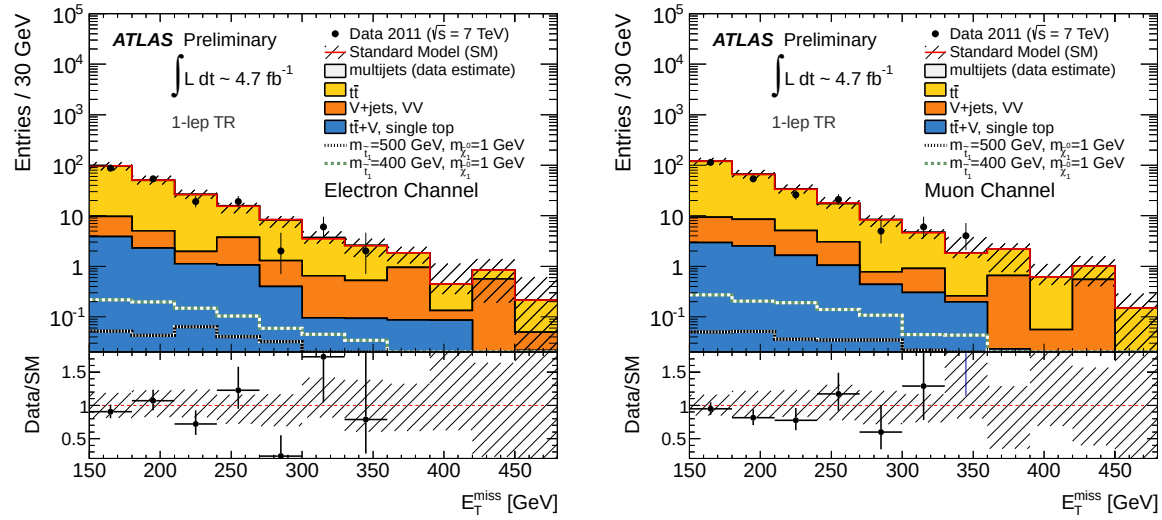

Figure 8: Electron (left) and muon (right) distributions of the missing transverse momentum ($E_{\mathrm{T}}^{\mathrm{miss}}$), in the 1-lepton top control region (1-lep TR).

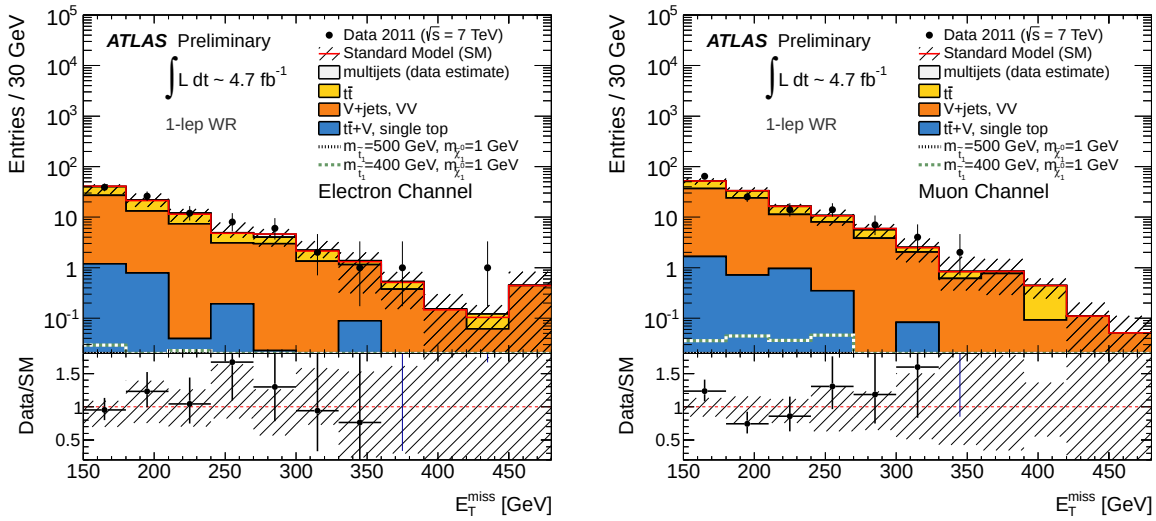

Figure 9: Electron (left) and muon (right) distributions of the missing transverse momentum ($E_{\mathrm{T}}^{\mathrm{miss}}$), in the 1-lepton W control region (1-lep WR).

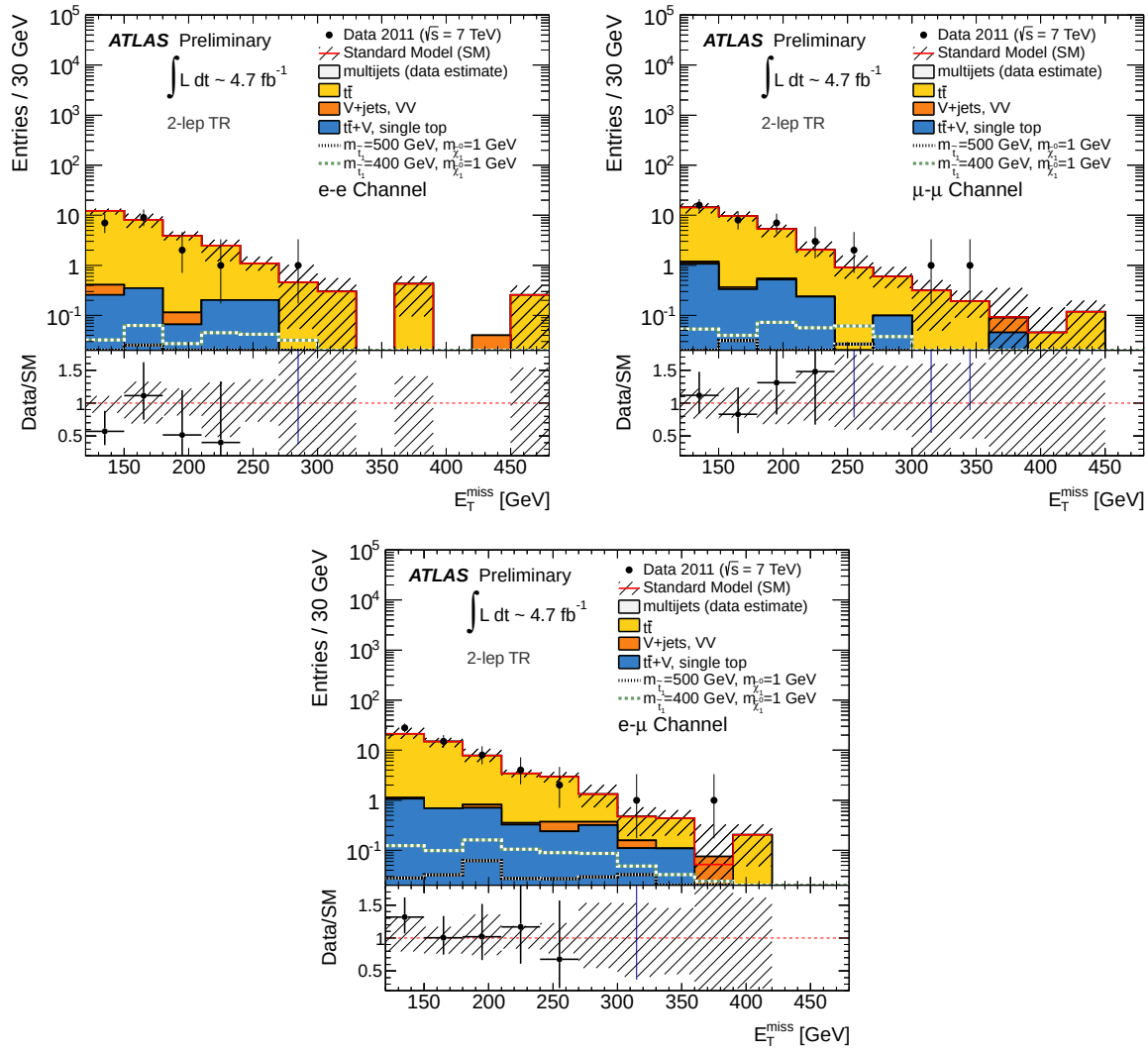

Figure 10: Missing transverse momentum ($E_{\mathrm{T}}^{\mathrm{miss}}$) in the 2-lepton top control region. The plots show the electron-electron (top left), muon-muon (top right), and electron-muon (bottom) channels.